Relevance of acoustic methods to quantify bedload transport and bedform dynamics in a large sandy-gravel bed river

Jules Le Guern[1], Stéphane Rodrigues[1,2], Thomas Geay[3], Sébastien Zanker[4], Alexandre Hauet[4], Pablo Tassi[5,6], Nicolas Claude[5,8], Philippe Jugé[7], Antoine Duperray[1], Louis Vervynck[1].

[1]UMR CNRS CITERES, University of Tours, France.
[2]Graduate School of Engineering Polytech Tours, University of Tours, France.
[3]BURGEAP R&D, Grenoble, France.
[4]EDF, Division Technique Générale, Grenoble, France.
[5]EDF R&D – National Laboratory for Hydraulics and Environment (LNHE), Chatou, France.
[6]Saint-Venant Laboratory for Hydraulics, Chatou, France.
[7]CETU Elmis Ingénieries, University of Tours, Chinon, France.
[8]EDF, Centre Ingénierie Hydraulique, La Motte Servolex, France.

Correspondence to: Jules Le Guern (leguern@univ-tours.fr).

Abstract

Despite the inherent difficulties in quantifying its value, bedload transport is essential for understanding fluvial systems. In this study, we assessed different indirect bedload measurement techniques with a reference direct bedload measurement in a reach of a large sandy-gravel bed river. Acoustic Doppler Current Profiler (aDcp), Dune Tracking Method (DTM) and hydrophone measurement techniques were used to determine bedload transport rates by using calibration with the reference method or by using empirical formulas. This study is the first work which attempted to use a hydrophone to quantify bedload rates in a large sandy-gravel bed river. Results show that the hydrophone is the most efficient and accurate method for determining bedload fluxes in the Loire River. Although further work is needed to identify the parameters controlling sediment self-generated noise, the calibration procedure adopted in this study allows a satisfactory estimation of bedload transport rates. Moreover, aDcp and hydrophone measurement techniques are accurate enough to quantify bedload variations associated with dune migration.

1. Introduction

Worldwide, rivers are in crisis (Vörösmarty et al., 2010). While changes in flow characteristics and fragmentation are well known (Grill et al., 2019), the impacts of human activities on the sediment budgets are yet underrepresented (Kondolf et al., 2018). The quantification of bedload transport is a key element to understand, manage and restore the physical and ecological functioning of fluvial systems. It is a prerequisite to an accurate estimation of global sediment budgets delivered by rivers to oceans (Syvitski and Milliman, 2007), to better understand bedform dynamics in river channels (Best, 1988; Bertoldi et al., 2009; Rodrigues et al., 2015; Claude

et al., 2014) and to reproduce satisfactorily morphodynamic processes with numerical modelling (Mendoza et al. 2017; Cordier et al., 2020).

However, in large rivers, this parameter remains difficult to estimate mainly due to human and material resources required to collect accurate measurements. Among the available tools, indirect measurement techniques are promising alternatives to direct measurements that are often cumbersome to implement, and can be time-consuming and perilous (Gray et al., 2010). Since the 2000s, numerous studies have been carried out to process the signal captured by acoustic Doppler current profilers (aDcp) as a tool for determining the apparent bedload velocity (Rennie et al., 2002; Rennie and Villard, 2004; Rennie and Millar, 2004; Kostaschuk et al., 2005; Villard et al., 2005; Gaeuman and Jacobson 2006; 2007; Holmes et al., 2010; Ramooz and Rennie, 2010; Latosinski et al., 2017; Conevski et al., 2019; Conevski et al., 2020a). The use of passive acoustic instruments has also been widely used to quantify bedload transport. Even though these latter techniques have been developed through the application of measurement tools such as geophones or hydrophones, their domain of applicability is restricted to the study of rivers with coarse sediments (Barton et al., 2010; Hilldale et al., 2014; Marineau et al., 2016; Geay et al., 2017). This study aims to develop the use of passive acoustic technique in large sandy-gravel bed rivers for quantifying bedload rates and bedforms dynamics.

In sandy-gravel bed rivers, the presence of bedforms is generally used to indirectly estimate bedload transport (Simons et al., 1965). Single beam (Peters, 1978; Engel and Lau, 1980) or multibeam echosounders (Nittrouer et al., 2008; Leary and Buscombe, 2020) are tools usually adopted to determine morphological parameters (such as bedform height, wavelength and celerity) or to estimate sediment budget (Frings et al., 2014). These bathymetrical surveys are often carried out simultaneously with sediment sampler measurements (Gaeuman and Jacobson, 2007; Claude et al., 2012) to calibrate the signal with a direct reference although the latter are intrusive and characterized by a low spatial representativeness. These drawbacks can therefore limit the applicability of these measurement techniques, in particular for large lowland rivers.

In this work, we compare the efficiency of active and passive acoustic techniques to quantify bedload transport. The investigation took place in a reach of the Loire River (France), which is characterized by a sandy gravel bed evolving through bars and superimposed dunes migration (Le Guern et al., 2019b).

The main objectives of this study were: 1) to compare indirect methods for estimating bedload with bedload estimates based on physical samples; 2) to estimate the accuracy of acoustic methods to measure cross sectional variations of bedload fluxes for various discharge conditions; and 3) to investigate the capabilities of hydrophones and aDcps at capturing bedload variations along bedforms.

2. Study site

The study site is located near Saint-Mathurin-sur-Loire, in the lower reach of the Loire River (France), approximately 150 km upstream of the mouth of the Loire River. The study reach is 2.5 km long, 500 m wide, nearly straight, with a bed slope of 0.02 % (Fig. 1). During this work we measured the grain size distribution and flow characteristics at different locations along a cross section (Fig. 1). The riverbed is composed of a mixture of siliceous sands and gravels with a median diameter (D_{50}) of 0.9 mm. The D_{50} varies between 0.3 and 3.1 mm with a standard deviation of 0.4 mm. The 90th percentile of the sediment grain size distribution (D_{90}) is variable with a median value of 3.3 mm varying from 0.5 to 15.7 mm. Hydraulic conditions varied according to discharge between 0.5 and 5.4 m for the water depth, and between 0.2 and 1.4 m.s^{-1} for the water velocity (median water depth and water velocity are 1.9 m and 0.9 m.s^{-1}, respectively). The width-to-depth ratio ranges from 120 to 550 depending on discharge variations. The mean annual discharge at the Saumur gauging station (approx. 30 km upstream) is 680 m^3.s^{-1}, with a 2-years flood of 2700 m^3.s^{-1}. Surveys were conducted during various hydrological conditions, with flow discharges ranging from 200 to 2400 m^3.s^{-1} (Fig. 2a).

Bars are characterized by an average wavelength of 1300 m, corresponding to approximately three times the channel width. The mean bar height is 1.5 m. At submerged conditions, bars can migrate with a celerity of 0.5 to 2 meters per day. During floods, the bar celerity can increase up to 4 meters per day (Le Guern et al., 2019a). During floods, dunes are superimposed on bars, whose height, wavelength and mean celerity are approximately 0.3 m, 4.4 m and 32 meters per day, respectively.

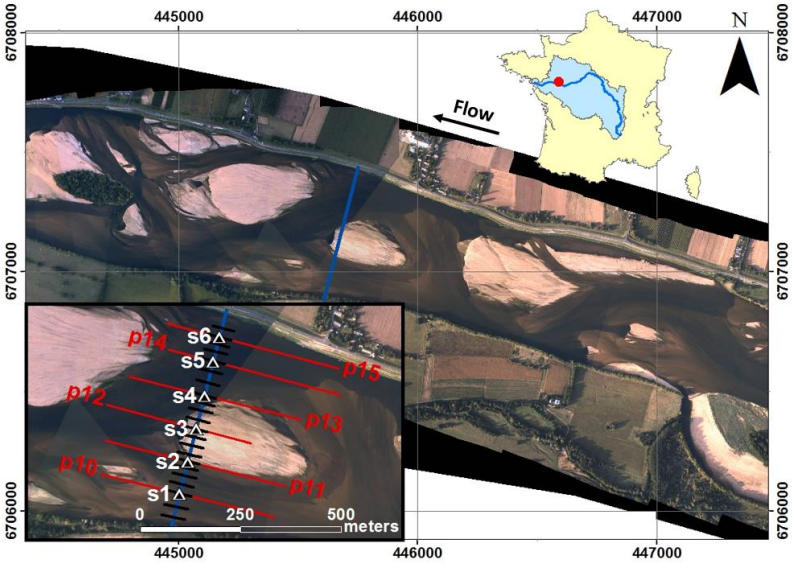

Fig. 1: Aerial photographs of the study site in 2017 (courtesy of Dimitri Lague, University of Rennes, France) with location of sampling points (white triangles) on the sediment transport gauging cross section (blue line), bathymetric profiles (red lines) and hydrophone drifts (black lines).

3. Materials and methods

Direct measurements of bedload sediment transport rates were performed using pressure-difference samplers. This conventional approach was used to evaluate three indirect acoustic methods: the apparent bedload velocity assessed from aDcp measurements, the dune tracking method (DTM) inferred using single-beam echosounding, and the self-generated noise (SGN) of sediments measured using a hydrophone. A total of 72 surveys were performed from October 2016 to May 2020 (discharge ranging between 210 $m^3.s^{-1}$ and 2290 $m^3.s^{-1}$) including 43 surveys with bedload samplers presented on Fig. 2a (Appendix A).

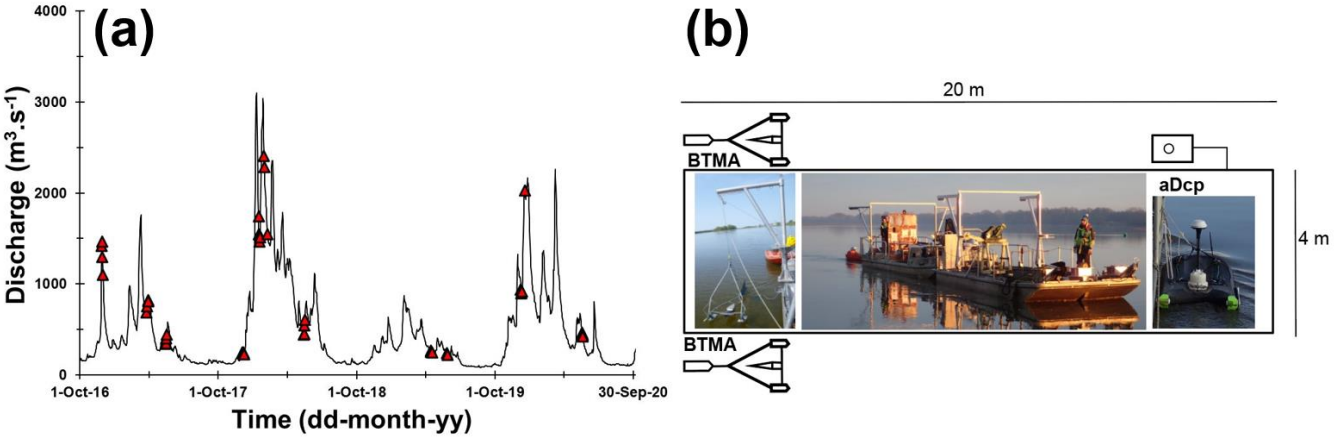

Fig. 2: (a), distribution of bedload sampling surveys along the hydrograph of Saumur gauging station located about 30 km upstream the study site. (b), Scheme of the main boat and disposition of monitoring facilities. Bedload Transport Meter Arnheim (BTMA) samplers; Acoustic Doppler Current Profiler (aDcp).

3.1. Bedload rates obtained using pressure-difference samplers

Bedload transport rates were measured using two synchronized Bedload Transport Meter Arnheim (BTMA) samplers, consisting of a sampling basket mounted on a frame. The sampling baskets have a rectangular mouth of 0.05 m high and 0.085 m wide. Complete description of the sampler can be found in de Vries (1979) or in Eijkelkamp (2003). Devices were mounted on a 20 meter-long boat stabilized using two anchors (Fig. 2b). These two samplers were deployed on 6 sampling points (S1 to S6) distributed along a cross section (Fig. 1). At each sampling point, 10 samples were collected with each BTMA (20 in total) and volumes of each samples were measured *in situ* with a graduated cone (Imhoff cone). Collected volumes were integrated over at least 2 minutes. All samples volumes from each BTMA were merged for sieving analysis (leading to 2 sediment samples per sampling point; one for each BTMA). Then, the average volume of caught sediments from the 2 BTMAs was computed and converted into instantaneous unit bedload rates as follow:

$$q_s BTMA = \frac{V}{b}\ \alpha\ \varepsilon\ \rho_s \times 10^3; \quad (1)$$

where $q_s BTMA$ is the unit bedload transport rate (g.s^{-1}.m^{-1}), α is the trap efficiency factor based on calibration (α=2), V is the mean volume of the instantaneous sediment catch (m^3.s^{-1}), b is instrument's mouth width (b=0.085 m), ρ_s is the sediment density (2650 kg.m^{-3}) and ε is the volumetric sediment concentration (assumed to be equal to 0.65). Suggested values of α and b were adopted from Boiten (2003) which mentioned that the trap efficiency factor does not include the possible losses of sediment finer than 0.3 mm (mesh size opening). Sampler positions and sampling quality were controlled by using two cameras mounted on the BTMAs but records during flood events were unusable. The increase of the water depth limits the light at the bottom of the water column and the addition of a mounted light did not improve the visibility because of particles in suspension. Sediment samples were analysed using the standard sieving technique (Folk and Ward, 1957) to determine the grain size distribution (GSD) using the tool "GRADISTAT" developed by Blott and Pye (2001). Uncertainties associated to the estimation of the unit bedload were calculated following Frings and Vollmer (2017).

3.2. Apparent bedload velocity from aDcp

Simultaneously with the BTMA measurements, an aDcp was installed on the boat (Fig. 2b). Measurements were performed using a Sontek Riversurveyor M9 (bi-frequency, 1 and 3 MHz) or a Teledyne RD Instruments Rio Grande (1.2 MHz). The sampling time needed to get a stable apparent velocity is in the range of 3 min for the case without bedforms (Conevski et al., 2019) and 25 min (Rennie et aI., 2002). In our study the sampling time was between 5 and 190 minutes. The aDcp was coupled with a RTK GPS Magellan ProFlex 500 receiving position corrections via the Teria network (centimeter level accuracy). The aDcp measurement allowed the use of both empirical approach and calibration approach for comparison with sediment sampler measurements. The apparent bedload velocity V_a was estimated from the bottom tracking signal, allowing the identification and the position of the river bed. In case of a mobile bed, the Doppler shift of the backscattered acoustic pulse of the bottom track depends on the boat velocity and to the bed velocity. According to Rennie et al. (2002), the apparent bedload velocity can be estimated using:

$$V_a = V_{GPS} - V_{BT}; \quad (2)$$

where V_{GPS} and V_{BT} are the boat velocity according to GPS reference and bottom track respectively. Even if the boat was anchored, the GPS signal was used in the Eq. 2 to correct apparent bedload velocity from small lateral displacements observed. When the GPS signal was poor or missing, V_{GPS} was considered as null and V_a resulted only from the bottom track signal V_{BT} (representing 15% of the dataset). Following Jamieson et al. (2011), the apparent velocity V_a was calculated for the North and East velocity components (respectively $\overrightarrow{V_{aE}}$ and $\overrightarrow{V_{aN}}$), limiting the over estimation especially in areas where inconsistent directions and low magnitudes of bedload velocity were found: $V_a = \sqrt{\overrightarrow{V_{aE}^2} + \overrightarrow{V_{aN}^2}}$.

To avoid compass and GPS issues, and to eliminate the effect of residual lateral displacement of the anchored boat, the apparent bedload velocity was projected onto the flow direction using:

$$V_{a\,proj} = V_a \cdot \cos\left(\frac{w_{dir\,BT} - b_{dir\,BT}}{180} \cdot \pi\right); \quad (3)$$

with $w_{dir\,BT}$ the flow direction with bottom track reference and $b_{dir\,BT}$ the boat direction with the bottom track reference (in degree). Equation (3) gives a value of apparent bedload transport velocity for each time step (approximately equal to 1 s) that was averaged to obtain a value for each sampling point. This method assumes that bedload is orientated in the same direction as the main flow. According to Rennie et al. (2002), the bedload transport rate per unit width ($q_s ADCP$, g.s^{-1}.m^{-1}) can be computed from two different kinematic models, the first of which is:

$$q_s ADCP = \frac{4}{3}\,\rho_s\, r\, V_{a\,proj} \times 10^3; \quad (4)$$

where r =D_{50}/2 is the particle radius, D_{50} is the median sediment diameter (m), ρ_s is the sediment density (2650 kg.m^{-3}). In this model, it is assumed the maximum bedload thickness is a single particle. The second model is:

$$q_s ADCP = V_{a\,proj}\; d_s\, c_b\, \rho_s; \quad (5)$$

where c_b is the concentration of the active transport layer considered as the saltation height (van Rijn, 1984), and the van Rijn (1984) formulation was adopted to compute the active layer thickness (d_s) as a function of the hydraulic condition and sediment grain size:

$$d_s = 0.3\, D_*^{0.7}\, T^{0.5}\, D_{50}; \quad (6)$$

$$c_b = 0.18\, \frac{T}{D_*}\, c_0; \quad (7)$$

$$T = \frac{\left(u_*'\right)^2 - (u_{*cr})^2}{(u_{*cr})^2}; \quad (8)$$

$$u_*' = \frac{\bar{u}}{5.75\log\left(\frac{12d}{3D_{90}}\right)}; \quad (9)$$

where c_0 is the maximum bedload concentration (0.65), T is the transport stage parameter that reflects the sediment mobility, u_*' is the bed shear velocity related to the grain (m.s^{-1}), d is the mean water depth (m), $\bar{u}$ is the mean flow velocity measured from the aDcp (m.s^{-1}) and u_{*cr} is the critical bed shear velocity (m.s^{-1}) calculated from the Shields curve (Van Rijn, 1984) and function of grain size through the scaled particle parameter D_*:

$$D_* = D_{50}\left[\frac{(s-1)g}{v^2}\right]^{\frac{1}{3}}; \quad (10)$$

where g is the acceleration of the gravity (m.s^{-2}), v is the kinematic viscosity (m^2.s^{-1}) and s the sediment density ratio. For the range of grain size of this study, u_{*cr} is computed as follows:

$$10 < D_* \leq 20;\; u_{*cr} = \left[0.04\, D_*^{-0.1}(s-1)gD_{50}\right]^{0.5}; \quad (11)$$

$$20 < D_* \leq 150;\; u_{*cr} = \left[0.013\, D_*^{0.29}(s-1)gD_{50}\right]^{0.5}; \quad (12)$$

In order to evaluate the sensibility of the apparent bedload post-processing, the two kinematic models (Eq. 4 and Eq. 5) were tested using raw apparent bedload velocity (V_a) and projected apparent bedload velocity ($V_{a\,proj}$).

To assess the capability of the aDcp to detect bedforms through the evolution of apparent bedload velocity, 3 surveys were conducted by positioning the aDcp 0.6 m above the river bed. This experimental scheme was adopted to avoid lateral movements of the boat, to be as close as possible to the river bed, and to reduce the space between beams. This configuration permitted us to fix the footprint for each beam to about 0.0046 m² and a distance of 0.56 m between opposed beams. This allowed us to describe the apparent bedload velocity with a finer accuracy especially in the presence of bedforms of 0.2 m height and 3.9 m long (in average). These surveys were performed for several hours (from 2.1 h to 4.7 h) to capture the migration of more than one dune lee side passing under the device. The value of apparent bedload velocity was smoothed by using a moving windows with an average of 500 points (approximately 500 seconds) to remove the outliers from the raw dataset. In the present study, all negative values were excluded from the comparison with BTMA measurements (16% of apparent velocity values).

3.3. Bathymetrical echosounding and dune tracking method

A single beam echosounder Tritech PA500 (0.5 kHz) coupled with a RTK GPS LEICA Viva GS25 was used for high-frequency bathymetric surveys to determine bar and dune morphodynamics along 6 longitudinal profiles (about 400 m long) centred on sampling points indicated in Fig. 1. Dune height (H_D) and wavelength (λ_D) were estimated using the Bedform Tracking Tool (BTT) based on the zero-crossing method (Van der Mark and Blom, 2007). Dune celerity (C_D) was estimated with the Dune Tracking Method (DTM, Simons et al., 1965; Engel and Lau, 1980) following the dune crests between two subsequent bathymetric surveys for a mean interval time equal to 40 minutes. The interval time needs to be adjusted with discharge because of the dune celerity variation from one survey to another. The determination of a proxy to evaluate sediment transport directly from DTM measurements is difficult because dune migration is function of several parameters. A semi-empirical equation that accounts for these parameters was used to compare bedload transport rates with the reference measurement. The computed dune parameters were used to calculate the unit bedload transport rate ($q_s DTM$, $g.s^{-1}.m^{-1}$) using the formula by Simons et al. (1965):

$$q_s DTM = (1-\lambda)\, \rho_s\, H_D\, C_D\, \beta \times 10^3; \quad (13)$$

where H_D is the mean dune height along the profile (m), C_D is the median dune celerity ($m.s^{-1}$) and β is the bedload discharge coefficient equal to 0.5 for a perfect triangular dune shape. The β coefficient neglects the volume of bypassing material from previous dunes or exchanges between bedload and suspended load (Wilbers, 2004). Due to its large variability (Van den Berg, 1987; Ten Brinke et al., 1999; Wilbers, 2004), the sensibility of the bedload transport rate was assessed for β=[0.33; 0.57], as proposed by Engel and Lau (1980) and Wilbers (2004). Considering the accuracy of the bathymetrical echosounding relative to the dune size, the sinuosity of dune crests, and the representativeness of dune celerity, only profiles with a mean dune height greater than 0.1 m and more than 10 dunes were considered.

3.4. Hydrophone and acoustic power

Passive acoustic monitoring was performed with a Teledyne RESON Hydrophone TC4014-5 (sensitivity of -180 dB) plugged into an EA-SDA14 card from RTSYS Company. This device has a large frequency range from 0.015 to 480 kHz, with a linear response until 250 kHz (±3dB). The beam-pattern of the hydrophone is omnidirectional. The hydrophone has been deployed following the protocol proposed by Geay et al. (2020). Longitudinal profiles were defined on the sediment transport sampling section (22 profiles see Fig. 1). The boat was positioned upstream of the sediment transport gauging section and left adrift at flow velocity. Depending on the water depth, the hydrophone was installed at a constant depth between 0.4 and 0.7 m below the water surface. Data acquisition was stopped after the boat crossed the sediment transport gauging section. The drift duration ranged between 15 to 140 seconds, depending on the flow velocity (mean time of 31 s). For each drift, a spectral probability density (SPD) was computed (Merchant et al., 2013). Then, a median Power Spectral Density (PSD) was computed as proposed by Geay et al. (2017). Median PSD are preferred to mean PSD as it filters out anomalous acoustic events such as the hydrophone impinging the riverbed. The acoustic power (P) for each drift was computed by integrating the median PSD over a range of frequency comprised between f_{min} (15 kHz) and f_{max} (350 kHz) (Geay et al., 2020):

$$P = \int_{f_{min}}^{f_{max}} PSD(f)\, df \; ; \qquad (14)$$

The minimum frequency was chosen to avoid hydrodynamic and engine noises, while the maximum frequency was set by the upper limit frequency of the device and was adjusted related to PSD. Finally, the nearest hydrophone drift for each BTMA sampling point was selected. Hydrophone drifts and sampler measurements were not synchronized. Several tests were carried out to ensure that these acoustic power variations were not related to the distance between the hydrophone and the river bed. As no theoretical expression has been developed to estimate bedload rates from hydrophone measurements, only the calibration approach was implemented.

4. Results

4.1. Comparison between acoustics and direct bedload transport rate measurements

The BTMA dataset is composed of 135 unit bedload rates calculated from 2628 individual sediment samples. This dataset represents an average of 19 samples on each sampling point to compute unit bedload rates (minimum of 5 and maximum of 57 samples). Bedload rates measured using the BTMAs ranged between 0.01 and 268 $g.s^{-1}.m^{-1}$. The standard deviation of unit bedload rates increased with discharge with a mean value of 33 $g.s^{-1}.m^{-1}$. This illustrates the spatio-temporal variability of sediment transport induced by bedform migration.

The aDcp dataset is composed of 96 simultaneous measurements of apparent bedload velocity and BTMA samplings (Fig. 3 and Appendix B). The mean apparent bedload velocity is 0.02 $m.s^{-1}$ and the maximum value was

0.11 m.s^{-1}. A Reduced Major Axis (RMA) regression has been computed between these two variables with a coefficient of determination (COD) R^2 equal to 0.51:

$$q_s = 1456\,V_a - 2.44; \quad (15)$$

As shown in Fig. 3, this site-specific calibration procedure at a reach of the Loire River is consistent with the dataset already published on several world large rivers (Rennie et al., 2017).

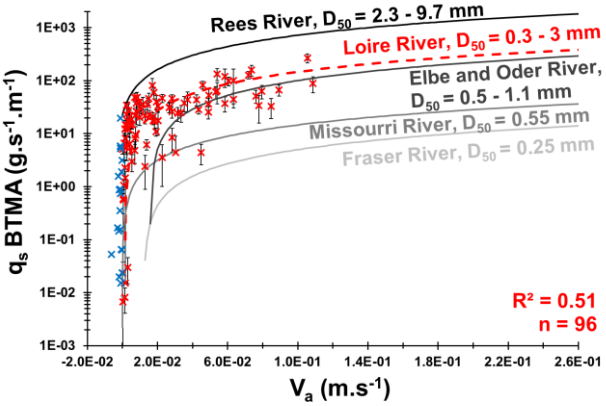

Fig. 3: unit bedload transport rates measured with BTMA samplers as a function of the apparent bedload velocity measured with aDcp. Red dashed line represents the RMA regression of the Loire River. Comparison with other site-specific calibration curves (Conevski et al., 2020a; Rennie et al. 2017). Blue marks represent negative apparent bedload velocity values excluded from this regression.

To evaluate the accuracy of a method against a reference, the discrepancy ratio is classically employed in the literature (Van Rijn, 1984; Van den Berg, 1987; Batalla, 1997) and is defined as the ratio between the bedload rate estimated with the indirect method and the bedload rate using BTMA. Computed bedload layer volume concentration (Eq. 7) varies between 0.005 and 0.1 (0.03 in average). Bedload layer thickness (d_s) (Eq. 6) ranges between $1D_{50}$ and $7D_{50}$ ($5D_{50}$ in average). Bedload rates computed using Eq. (5) underestimate BTMA bedload rates with only 24% of the dataset with a discrepancy ratio between 0.5 and 2 (Fig. 4b). By considering apparent bedload velocity without projection onto the flow direction, the kinematic model (Eq. 5) estimates satisfactorily BTMA bedload rates with 41% of the dataset with a discrepancy ratio between 0.5 and 2. Conversely, using raw apparent bedload velocity in Eq. (4), leads to only 33% of the dataset varying with a factor of 2 against 54% with projected V_a (Fig. 4a). According to these results, Eq. (4) better describes the sampler bedload rates with projected apparent bedload velocity whereas raw apparent bedload velocity are preferred with Eq. (5). Some outlier data are observed for BTMA bedload discharge lower than 0.1 g.s^{-1}.m^{-1}. These points correspond to low flow conditions for which bedload samplers could under-estimate bedload fluxes (gap between the sampler mouth and the riverbed).

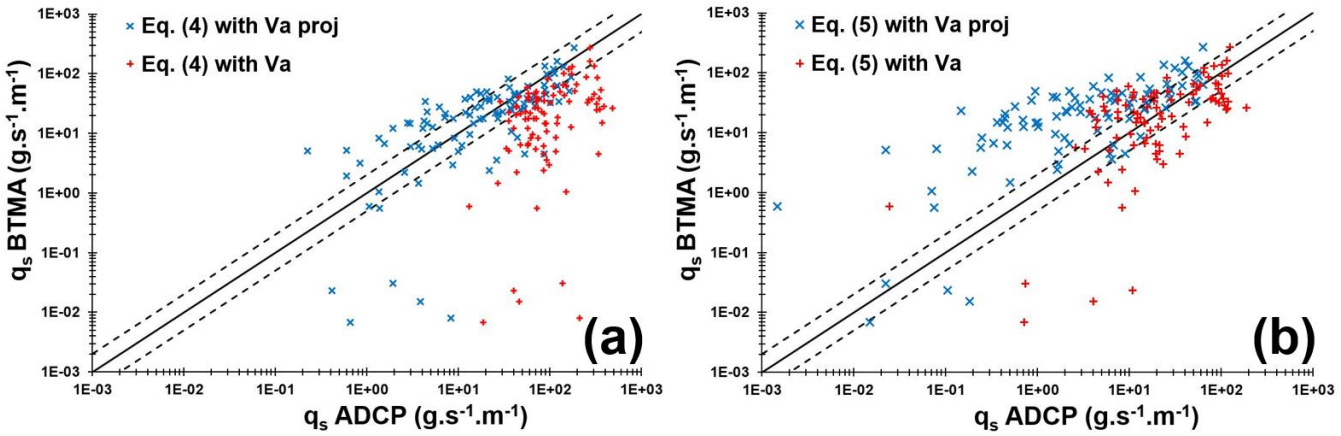

Fig. 4: log/log correlation between bedload rates measured with BTMA sampler and calculated using: (a) Eq. (4) and; (b) Eq. (5). Solid black line represents the perfect correlation and dashed black lines represents a factor of 2 above and below the perfect correlation.

It appears difficult to estimate bedload rates only from dune celerity by assuming a direct relation between dune celerity and bedload transport rates measured with BTMA. Estimation of bedload transport rates from dune morphology has been performed by using empirical formula of Simons et al. (1965) (Eq. 13). The dataset is composed of 49 DTM profiles with associated BTMA samples (Appendix C). The mean dune height and length vary from 0.1 to 0.5 m, and 1.3 to 12 m, respectively. The median dune celerity varies between 13 and 61 $m.d^{-1}$. According to Fig. 5a, bedload rates estimated with a discharge coefficient β = 0.33 are in agreement with BTMA bedload rates with 67% of values in a factor of 2 of the perfect correlation compared with 49% of values for a discharge coefficient of 0.57 (Fig.5a). The definition of the discharge coefficient proposed by Engel and Lau (1980) is better adapted for the observed dune shapes found in the Loire River which are characterized by mean steepness (H_D/L_D) approximately equal to 0.05 (in line with other observations on the Loire River, Claude et al., 2012; Rodrigues et al., 2015; Wintenberger et al., 2015).

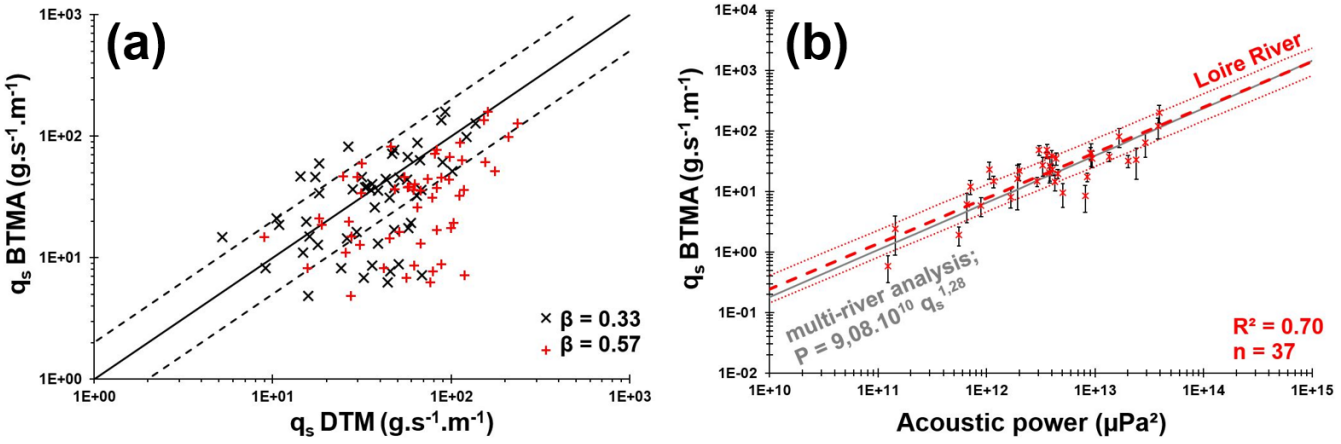

Fig. 5: (a), log/log correlation between bedload rates measured with BTMA samplers and bedload rates calculated using Eq. (13). Solid black line represents the perfect correlation and dashed black lines represents a factor 2 of the perfect correlation. (b), unit bedload rates measured with BTMA samplers as a function of acoustic power measured with hydrophone. Dashed red lines represents the RMA regression with envelopes curves of a factor 2 of the bedload rates. Comparison with Geay et al. (2020).

Even if the statistical representativeness is lower than other methods (n=37, Appendix D), the RMA regression between the acoustic power and BTMA sampling is better (R^2=0.70) and 60% of values varying between a factor 2 (Fig. 5b). In consequence, new equation to estimate sediment transport from acoustic power is proposed:

$$P=6.6 \times 10^{10} q_s^{1.32}; \quad (16)$$

This calibration curve is similar to observations performed by Geay et al. (2020) on 14 study sites distributed on 11 different rivers despite the use of different instruments (sampler and hydrophone) and the integration of median PSD over a wider range of frequency in the present study. Moreover, the median PSD differ from the Isère River (Petrut et al., 2018) and from Drau River (Geay et al., 2017). These rivers are characterised by coarser sediments (see Fig. 6a) and the central frequency of the PSD decrease with an increasing D_{50}. These observations are in line with Thorne's (1986) theory. The central frequency of the median spectrum of the Loire River is approximately equal to 140 kHz. The frequency band of the bedload is shifted towards high frequencies due to finer grain size.

The acoustic power corresponding to the integration of the spectrum over a range of frequency is related to the grain size (Thorne, 1985) and sediment kinematics (Gimbert et al., 2019). To analyse the effect of sediment mobility on the acoustic power, the transport stage parameter (Van Rijn, 1984) is calculated. The power law adjusted between these two parameters provides evidence for a positive evolution of the acoustic power with sediment mobility (Fig. 6b).

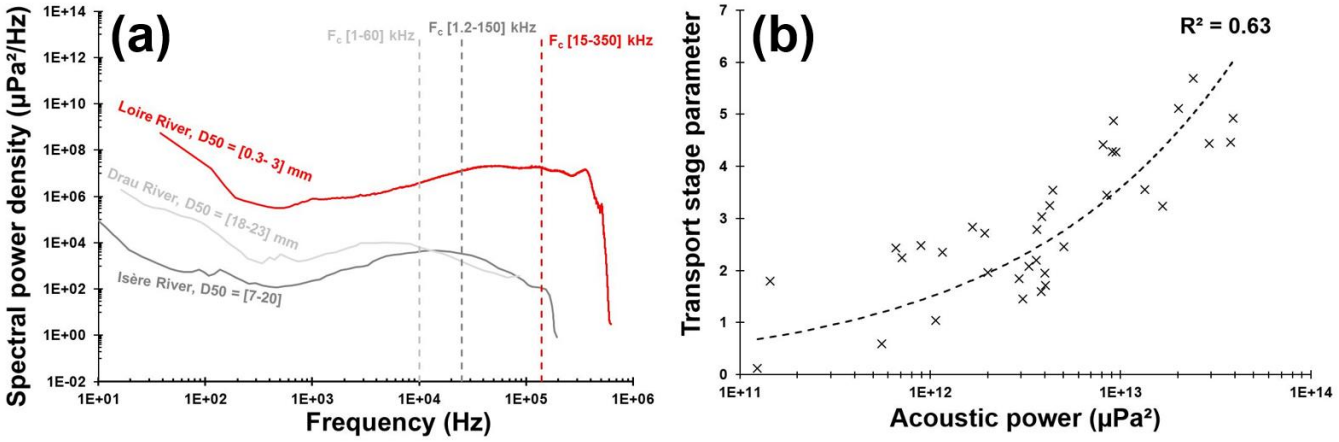

Fig. 6: (a), Comparison of PSD from 3 rivers with varying D_{50} (PSD of the Drau River and the Isère River are extracted from a single measurement, PSD of the Loire River is the median PSD from 450 measurements). (b), transport stage parameter (from Van Rijn, 1984) as a function of acoustic power.

The comparison can be performed between indirect methods to discuss the acceptability of the BTMA reference. The apparent bedload velocity and the acoustic power are poorly correlated with mean dune morphological parameters (Table 1).

Table 1: Coefficient of determination (COD) between dune parameters and acoustic methods (log values).

	P	V_a	$q_{s\ BTMA}$	H_D	C_D
H_D	0.20	0.27	0.16	-	-
C_D	0.22	0.24	0.36	0.22	-

The apparent bedload velocity estimated by aDcp is the velocity of the top layer velocity or dynamical active layer (sediment being transported over a dune), whereas the dune celerity is the mobility of the exchange event active layer, according to Church and Haschenburger (2017). It must be noted that apparent bedload velocity is higher than dune celerity by a factor approximately equal to 100. On the other hand, the apparent bedload velocity is positively correlated with the acoustic power. The COD of the RMA regression is equal to 0.76 (Fig. 7a).

Before focusing on the spatial distribution of unit bedload rates, total bedload rates are calculated by interpolating unit bedload rates between sampling points on the cross section for each method. The COD of the RMA regression established between BTMA bedload rates and water discharge is 0.71 (Fig. 7b) with 77% of the values varying within a factor of 2. The dispersion of bedload rates is higher for low water discharge (less than the mean annual discharge of 680 $m^3.s^{-1}$). Bedload rates are estimated from Eqs. (13), (15) and (16), for the DTM, the aDcp and the hydrophone, respectively. Both the hydrophone and DTM bedload rates are less scattered with 96% of values with a discrepancy ratio between 0.5 and 2, compared with 82% for the aDcp.

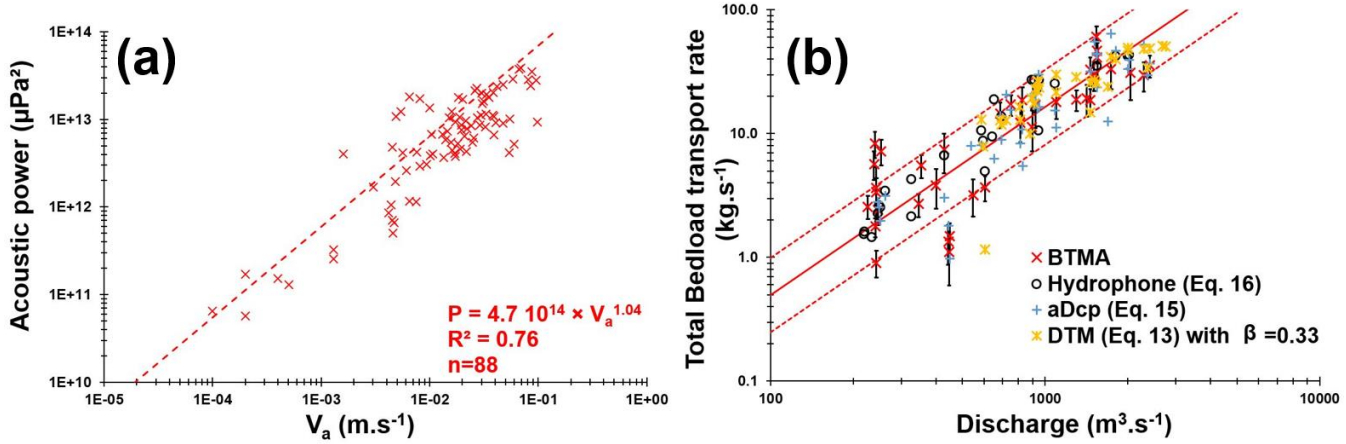

Fig. 7: (a), acoustic power as a function of apparent bedload velocity. (b), Cross section integrated bedload transport rates as a function of discharge.

4.2. Spatial distribution of bedload in a sandy gravel-bed river with migrating bedforms

4.2.1. Determination of bedload transport on a cross section using acoustics methods

To compare the spatio-temporal distribution of bedload transport rates, sediment transport sampling was performed on the same cross section for all surveys and for various discharge conditions. Two surveys with contrasting discharge conditions and different bed configurations are presented (Fig. 8) to illustrate the capability of acoustic methods to determine bedload active width in a river reach characterized by the presence of macroforms and superimposed mesoforms (*sensu lato,* Jackson, 1975).

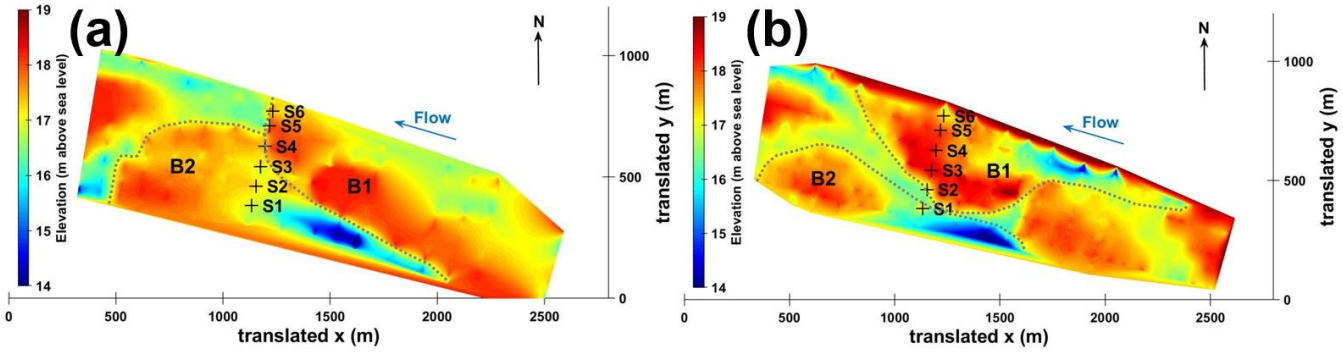

Fig. 8: Digital Elevation Models (obtained using natural neighbours interpolation of single beam bathymetrical surveys) showing location of sampling points with respect to bar location during: (a), survey of the 17/05/2018 (Q=604 $m^3.s^{-1}$) and (b), survey of the 19/12/2019 (Q=2050 $m^3.s^{-1}$).

In May 2018, a bar (B1. Fig. 8a) was located just upstream of the sediment gauging section from the center to the right part of the channel. In the left part of the channel, BTMA sampling was performed on the stoss side of another bar (B2, Fig. 8a). Consequently, bedload rates gradually rose from the center of the channel (2 $g.s^{-1}.m^{-1}$, S4) to the left part of the channel (15 $g.s^{-1}.m^{-1}$, S1) except for the DTM (Fig. 9a). The intensity of bedload transport rates was evaluated for each acoustic signal from regression equations established above (Eqs. 13, 15 and 16, for DTM, aDcp and hydrophone, respectively). The linear equation of aDcp calibration allow the calculation of negative bedload flux for apparent bedload velocity below 0.0016 $m.s^{-1}$ (Fig. 9a, S4). ADcp and hydrophone signals followed the same trend as the BTMA measurement. In the right part of the channel, no reference measurements were available (S5 and S6) but all acoustic signals followed the same trend (increasing bedload transport rates). The bedload rates estimated with the DTM were lower than the reference in the left part of the channel. This can be explained by the reduced number of dunes in this area that caused a higher uncertainty in dune celerity determination. In the right part, the proximity of the bar front induced lower bedload transport rates measured with aDcp and hydrophone. DTM integrates sediment dynamics over a longitudinal profile that does not necessarily reflect the bedload transport conditions at a local scale. Due to the lee effect provided by the proximity of the bar front, dunes were not present downstream of the bar and only dunes located on the stoss side of the bar were used

to calculate the mean dune celerity. ADcp underestimates whereas the hydrophone method overestimates the unit bedload rate compared with BTMA measurements.

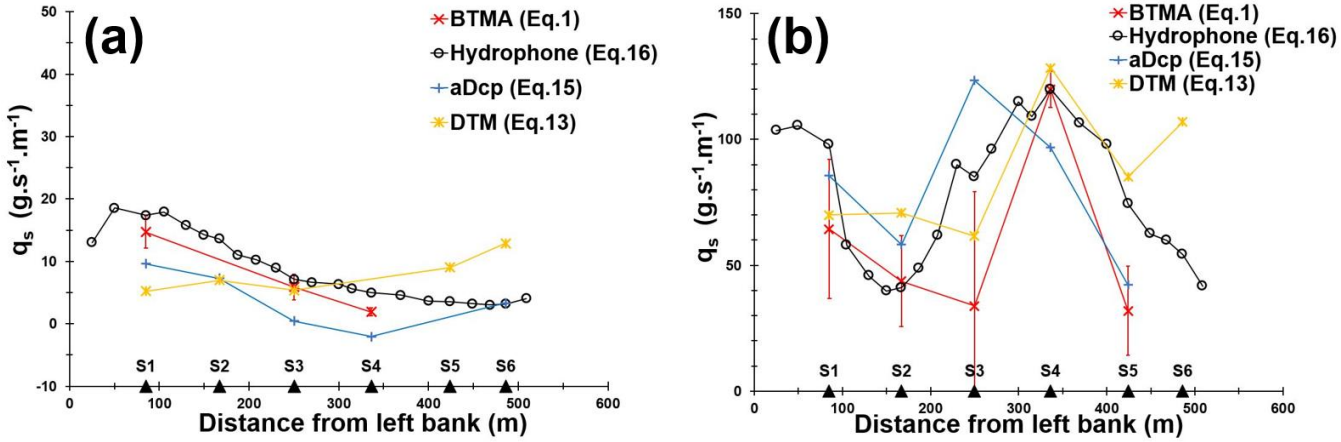

Fig. 9: Lateral distribution of unit bedload rates assessed from different methods for two surveys performed: (a), the 17/05/2018 (Q=604 m^3.s^{-1}) and (b), the 19/12/2019 (Q=2050 m^3.s^{-1}), respectively.

In December 2019 (Fig. 9b), the flow discharge was higher (2050 m^3.s^{-1}) than the value observed in May 2018 (Q=604 m3s-1) and measured bedload rates ranged between 32 and 120 g.s^{-1}.m^{-1}. Due to the bar migration, the bed configuration was different. Bar B1 reached the sediment gauging cross section. As a consequence, sampling points S3 to S6 were located on the stoss side of bar B1 (Fig. 8b). The sampling point S2 was located just downstream of the bar front where the velocity and sediment transport rates were lower (Fig. 8b). The high spatial resolution of the hydrophone measurements confirmed that the preferential bedload active width was located between 250 and 450 m from the left bank (Fig. 9b). For this survey, acoustic signals (*i.e.* acoustic power, apparent bedload velocity) followed the same evolution pattern as samplers along the cross section except for S3. Bedload transport rates determined with the DTM did not follow the trend of bedload rates determined with aDcp and hydrophone at the proximity of bar front and near the bank as in the previous survey (S2 and S6). The hydrophone model overestimated the sediment transport in comparison with the BTMAs for S1, S3 and S5.

4.2.2. Sediment transport processes on bedforms analyzed from aDcp and hydrophone

The aDcp computed bedload rates evolved according to bedform location for fixed measurements performed on dunes of height ranging between 0.05 m and 0.2 m (Fig. 10a and 10b). Higher bedload rates were found on the crest of the dune and lower values in the trough. The amplitude of bedload rates between crest and trough for low flow conditions (Fig. 10b) ranged between 42 g.s^{-1}.m^{-1} and 67 g.s^{-1}.m^{-1}. For higher flow conditions, it varied between 45 g.s^{-1}.m^{-1} and 91 g.s^{-1}.m^{-1} (Fig. 10a). These values were extracted considering bedload rates in trough as equal to zero (not negative). The aDcp linear regression (Eq. 15) did not allow the calculation of bedload transport rates due to negative apparent bedload velocity. This is the case downstream the lee face of dunes (Fig. 10a, between

8 to 42 min., 96 to 107 min., 185 to 193 min., and 227 to 230 min.; Fig. 10b, between 48 to 55 min. and 153 to 162 min.). The mean time recorded between two successive dune crests was 1 hour.

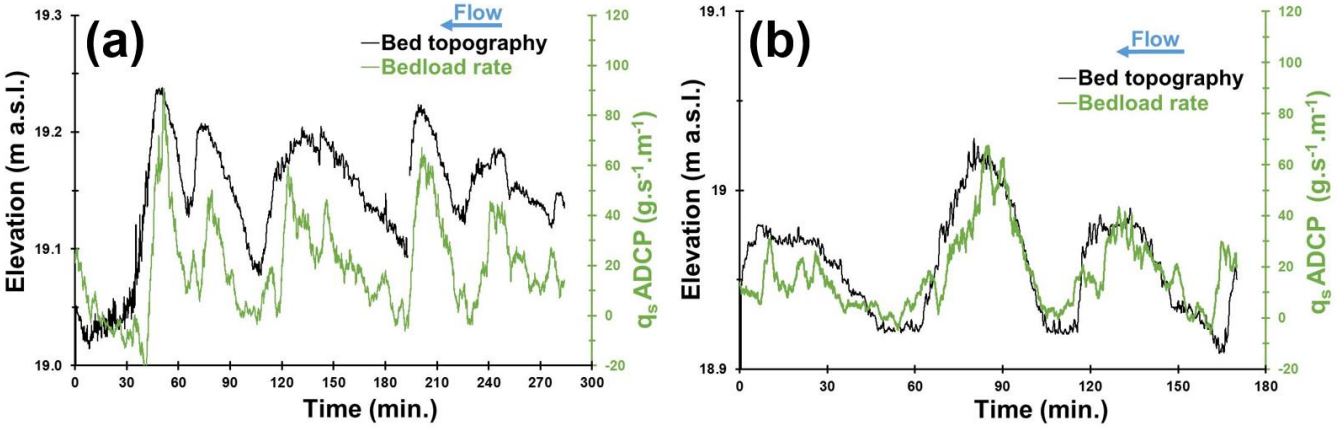

Fig. 10: Bedload rates calculated using Eq. (15) and bed topography obtained during a static measurement performed using an aDcp: (a), survey done on the 20/05/2020 (Q=470 $m^3.s^{-1}$; mean water depth = 1.04 m) and (b), survey done on the 29/05/2019 (Q=210 $m^3.s^{-1}$; mean water depth = 0.85 m).

Hydrophone drifts showed that the longitudinal evolution of acoustic power can be correlated with changes in elevation of the riverbed due to dune and bar presence. For instance, in the presence of a 2 meter high bar front, the bedload rate significantly decreased, illustrating the lee effect that is characterised by a decrease in bedload sediment transport (Fig. 11a). This shows that the hydrophone is sensitive enough to detect this local phenomenon induced by the presence of a bar front immediately upstream. The bedload rates range from about 8 $g.s^{-1}.m^{-1}$ on the bar crest to 376 $g.s^{-1}.m^{-1}$ in the bar trough (1 10^{12} µPa² to 1.7 10^{14} µPa² of acoustic power, respectively). According to flow velocity measurements, it appears that a 2 m high bar front can influence flow velocity and bedload transport rates up to the reattachment point located approximately 100 m downstream. Downstream of the bar front, the bedload transport rate increased at 11h06min (Fig. 11a) that would be in coincidence with the flow reattachment point. Further downstream, the bedload transport rate increased from 8.5 to 23.4 $g.s^{-1}.m^{-1}$ (representing respectively an acoustic power of 1.2×10^{12} µPa² to 4.1×10^{12} µPa²), where dunes exhibit a more regular shape increasing their amplitudes from 0.02 m to 0.4 m, approximately. On the left part of the channel (Fig. 11b), the drift was located at the stoss side of a bar where larger dunes were observed (about 1 m in height) with superimposed small dunes (height approximately equal to 0.3 m). The bedload transport rate calculated above these bedforms increased near the crests of the large dunes (about 80 $g.s^{-1}.m^{-1}$) and decreased in the troughs (about 50 $g.s^{-1}.m^{-1}$) where superimposed bedforms were smaller (Fig. 11b).

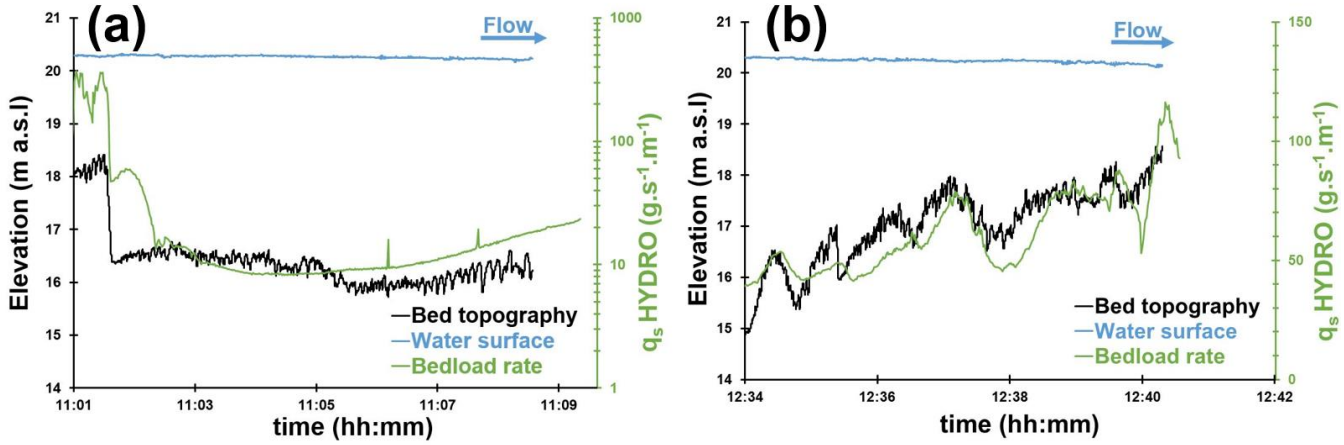

Fig. 11: Bedload rates calculated on bedforms using the hydrophone and Eq. (16) near a bar front (a) and on a dune field (b). Bed topography and water surface along two longitudinal bathymetric profiles for the 08/02/2018 survey, Q=1550 m^3.s^{-1}: (a), P10, mean water depth = 3.8 m. The profile length from 11:01 to 11:09 corresponds to 400 m; (b), P12, mean water depth = 3.4 m. The profile length from 12:34 to 12:41 corresponds to 518 m.

5. Discussion

5.1. Relevance of acoustics for computing bedload transport rates

Despite their lack of accuracy and their low spatial representativeness, samplers allow a direct measurement of bedload and represents the only reference measurement of bedload in the field. The presence of bars affect sediment transport locally and make sampling method very sensitive to the location of the sampling point. For low water discharge (below mean annual discharge, 800 m^3.s^{-1}), bars are emerged and reduce considerably the width where sediment transport occurs. The number of sampling point decreases with discharge (because bars were not flooded) leading to a higher bedload rates variability (Fig. 7b). Moreover, in weak bedload transport conditions, the BTMA sampler most likely performed with reduced efficiency initially calibrated to 50%, (van Rijn and Gaweesh, 1992; Gaweesh and van Rijn, 1994; Banhold et al., 2016). The presence of dunes influences the performance of the sampler by preventing the exact positioning of sampler mouth on the river bed. These deficiencies lead to a large uncertainty in bedload estimation which set the limits of the comparison with other methods.

The use of hydrophones to estimate bedload transport in a lowland sandy gravel-bed river constitutes a new research topic. As discussed by several authors, the use of hydrophones was so far restrained to gravel-bed rivers (Bedeus and Ivicsics, 1963; Barton et al., 2010; Hilldale et al., 2014; Thorne, 2014; Marineau et al., 2016; Geay et al., 2017) or marine environments (Thorne et al., 1984; Thorne, 1986; Blanpain et al., 2015). More recently, Geay et al. (2020) highlighted that the acoustic power measured with a hydrophone can be correlated to the sampler measurements of bedload in fluvial environments characterized by bed slopes varying between 0.05 and 2.5% and channel width ranging between 8 and 60 m. In these mountainous environments, the median grain size ranged

between 0.9 and 62 mm (n=582 samples). In our study, the downstream reach of the Loire River shows smaller slope (S=0.02%), a wider channel (W=500 m), and a median grain size ranging between 0.3 mm to 3.1 mm (n=450 samples). The hydrophone is therefore an efficient tool for sediment transport gauging, allowing the measurement of numerous sampling points (average of 17 sampling points) during a relatively shorter time period (one hour). This high spatial discretization makes the hydrophone functional over a wide range of discharges (even for low water discharge, Fig. 5b) by catching the high spatial variability of bedload transport. It should be pointed that the regression calculated in the present study (Eq. 16) is obtained from unit bedload rates (from several samples) and the acoustic power resulting to a unique acoustical drift, whereas Geay et al. (2020) compared averaged cross section bedload rates and acoustic power. Despite these differences, the data presented above corroborate the results by Geay et al. (2020) and support their conclusions concerning the determination of a global calibration curve between acoustic power and bedload rates by extending its application to the lowland sandy gravel-bed rivers. Although this needs to be confirmed by further investigations to better understand parameters that control the acoustic power measured (such as the propagation of sound waves in water (Geay et al., 2019) and their attenuation, the saltation length and associated impact celerity, or sediment grain size), results presented in this study suggest that the hydrophone method could be an efficient way to measure and to map bedload transport rates on a wider range of fluvial systems.

Several laboratory studies have been carried out (Ramooz and Rennie, 2010; Conevski et al., 2019; Conevski et al., 2020b) and rivers instrumented with aDcp to determine bedload rates (Rennie et al., 2002; Rennie and Millar, 2004; Gaeuman and Jacobson, 2006; Gaeuman and Pittman, 2010; Brasington et al., 2011; Conevski et al., 2020a). Recent works have been carried out on two rivers (Elbe, Oder) similar to the Loire River in term of grain size characteristics, flow and shear velocity, and water depth (Conevski et al., 2020a). Even if the correlation between apparent bedload velocity and bedload rates is significant, this calibration equation (Eq. 15) was obtained from two very similar rivers. Despite these observations, there is no general agreement between bedload rates and apparent velocity (Rennie and Villard, 2004; Rennie et al., 2017). The response of aDcp to bedload transport depends on several parameters The variation of the impulse frequency, the pulse length, beam focusing or associated internal signal processing (Broadband or Narrowband) can lead to different estimation of the apparent bedload velocity for the same sediment transport conditions (Conevski et al., 2020a). These parameters vary from a device to another (RDI/Sontek; Conevski et al., 2020b). As the aDcp pulse sample a volume of the riverbed (Rennie et al., 2002) which can lead to a biased estimation of V_a: *i*) an underestimation in case of large roughness of the riverbed with most of the reflected pulse is scattered by the immobile particles below the active layer (Conevski et al., 2019); *ii*) an overestimation in case of high concentration of the bedload layer (Rennie et al., 2017) or sand particles in suspension near to the riverbed (water bias, Rennie and Millar, 2004). Even if a general trend seems to be highlighted by the river comparison (Fig. 3) with an increasing bedload rate as grain size increases for a constant V_a, the relationship between grain size and V_a cannot be easily determined in response to all variables

mentioned above. One explanation of this trend could be that suspended sands could contribute to the bottom tracking signal without being caught by the sampler (Rennie et al., 2017). Moreover, the accuracy of the measurement on a single cross section depends on the water depth heterogeneity that in turn influences the aDcp footprint and makes the aDcp method location sensitive when bedforms are present (Fig. 9b). Estimation of bedload rates using empirical equations is limited by the number of variables that are difficult to measure in the field (e.g. thickness and concentration of active layer, Kostaschuck et al., 2005; Villard et al., 2005; Holmes, 2010; Latosinski et al., 2017; Conevski et al., 2018). The results shown in Fig. 4a suggest that Eq. (4) estimates sampler bedload rates if the projected bedload velocity is used. This kinematic model does not account for the thickness or the sediment concentration of the bedload layer and assumes that bedload transport never exceeds the size of a single particle assessed as uniform in terms of grain size (Rennie et al., 2002). These assumptions seem not to be appropriate for a sandy-gravel bed river. The active layer thickness should increase as suspended bed material load increases. Nevertheless, results are in agreement with BTMA bedload rates (Fig. 4a). This can be explained by an underestimation of the apparent bedload velocity when it is projected along flow direction. On the other hand, Van Rijn (1984) defined the bedload layer thickness equal to the saltation height. The computed values of bedload layer thickness are coherent with other estimations performed on comparable rivers (Conevski et al., 2020a). The Eq. (5) better estimates sampler bedload rates using the raw bedload velocity (Fig. 4b). If we consider that c_b and d_s are well estimated by van Rijn equations (Eqs. 6 and 7), these results confirm that the projection of the apparent bedload velocity decreases the bedload velocity magnitude when the bedload direction differs from flow direction (e.g. bed slope effects). The influence of bedload velocity projection appears to be important when bedload are computed using kinematic models. Nevertheless, the calibration curve seems to be in agreement with other studies. Although, the application domain of Eq. (4) does not correspond to the conditions in the Loire River, the decrease of projected V_a seems to compensate the overestimation of bedload rates when the raw apparent bedload velocity is used. This is the opposite for Eq. (5) that accounts for bedload layer thickness and sediment concentration. In this case, the projection of V_a leads to an underestimate of bedload rates. Further works need to be done to improve the post-processing of V_a by recently published filtering procedures (Conevski et al., 2019 and 2020a) and to estimate its effect on calibration curve and kinematic models.

Contrarily to the aDcp, the DTM allows the investigation of the “event active layer” (Church and Haschenburger, 2017). The DTM is not a punctual measurement of bedload. Consequently, in presence of macroforms such as bars, it is difficult to compare with BTMA samples because it takes into account dunes that are not necessarily present at the BTMA sampling point (typically downstream of a bar lee side). To some extent, the DTM and BTMA methods integrate bedload longitudinally at different scales. The presence of a local disturbance (or migrating bedform at low celerity) will affect the measurement. The determination of dune celerity by post-processing is time-consuming compared with the determination of dune morphology and the existing open access post-processing tools. In order to determine bedload rates with empirical equations, this method needs a calibration coefficient that

is difficult to measure in field studies (Ten Brinke et al., 1999; Wilbers, 2004). Moreover, physical samplers sample the dynamical active layer, thus are more comparable to the hydrophones and aDcps. Nevertheless, DTM remains an accurate method to estimate bedload transport in the Loire River (Fig. 5a) where dunes are present and high enough (over the mean annual discharge).

As suggested by previous authors, both aDcp (Kenney, 2006) and hydrophone (Bedeus and Ivicsics, 1963) allow a reliable representation of bedload fluxes on a cross section through the regressions with bedload rates obtained using samplers. Figures 9a and 9b highlight the benefits of the use of acoustic devices for the determination of bedload transport rates in a large sandy gravel-bed rivers. In the present study, the time needed in the field to complete the BTMA, DTM, aDcp and hydrophone methods (respectively the red, yellow, blue and black lines of Fig. 9b) are about 1 day, 4 hours, 1.5 hours and 45 minutes, respectively. These times were estimated including the time needed to position and anchor the boat at each sampling point. This underlines the high potential of hydrophones to quantify bedload in large rivers with high spatial variability of sediment transport and map bedload sediment fluxes at a large scale as proposed by Williams et al. (2015) using the aDcp. Moreover, all indirect methods tested here seem to be able to quantify total bedload transport as efficiently as the direct method (Fig. 7b) but special care should be taken with local estimation of bedload rates (Fig. 9a and Fig. 9b).

Finally, regarding the correlation of aDcp and hydrophone with BTMA (Fig. 3 and Fig. 5b), we can raise the question of the reference method. Indeed, the regression between aDcp and hydrophone is more significant (R^2=0.76) and it could be the quality and the accuracy of BTMA sampling that reduce the quality of indirect measurement regressions.

5.2. Hydrophone and aDcp sensitivity to bedform observations

Passive (hydrophone) and active (aDcp) acoustic devices are rarely used to analyse of the bedload transport rates associated with bedforms in relatively large lowland rivers. Several studies mention differences in apparent bedload velocity according to the location on bedforms (Rennie and Millar, 2004; Villard and Church, 2005; Gaeuman and Jacobson, 2006; Holmes, 2010; Latosinski et al., 2017). These authors have shown that apparent bedload velocity increases from trough to crest of the dune and confirmed previous observations made with samplers (Kostachuck and Villard, 1996; Carling et al., 2000). These observations were made on large dunes that migrate too slowly to allow a continuous measurement along bedforms. Our study complements these observations by providing a fixed and continuous measurement of apparent bedload velocity and providing bedload transport rate estimation based on a calibration curve. The mean time between two subsequent crests (1 hour) shows that even for small bedforms (H_D = 0.05 to 0.2 m, Fig. 10a and Fig. 10b), the aDcp location significantly influences the bedload rates calculated over a dune field (0.03 to 0.08 $m.s^{-1}$ of difference between crest and trough). This suggests that care should be taken using this method on river beds where large dunes are present but also when small dunes are migrating. According to Rennie and Millar (2004), the sampling area diameter increases with the water depth and is

approximately equal to flow depth. Our protocol minimizes the water depth by submerging the aDcp and therefore minimizes the beams sampling diameter, hence, minimizes the probability of sampling stoss or lee sides of the same dune simultaneously.

In our study context, the acoustic power recorded by the hydrophone was not affected by the distance between the hydrophone and the river bed. To our knowledge, there are no references mentioning investigations on bedload transport rates associated with bedforms using a hydrophone. At a large time step (mean aDcp and hydrophone samples), the apparent bedload velocity and the acoustic power did not follow the observed trend of mean bedform characteristics derived from DTM measurement (dune celerity and dune height). This could be explained by the difference of spatial scales between DTM and other methods. For a smaller time step, our results showed that acoustic power is able to describe the influence of bars on bedload sediment transport (Fig. 11a). Moreover, as for the aDcp, the hydrophone also detects the theoretical pattern of bedload transport rates associated with bedform migration. As shown by Reesink et al. (2014), the lee effect generated by bar fronts influences the development of dunes downstream. Specifically, the hydrophone is able to record the decrease of the acoustic power immediately downstream of the bar front and its progressive increase downstream (translated by the development of dunes at about 11h06, Fig. 11a). In the present study, dunes smaller than 0.4 m (Fig. 11a) were not high enough to allow the observation of changes in the acoustic power along the bedform stoss sides. On the contrary, for higher dunes (H_D = 1 m, Fig. 11b) the bedload generated noise can be well recorded by the hydrophone. A hydrophone senses all noises that are propagating in the water column. Therefore, the hydrophone can record noises that are far away from its location. Noises are more and more attenuated with increasing distance (Geay et al., 2019). Particularly, when there is few bedload noise close to the hydrophone, the hydrophone can sense the bedload noise that are generated far away. This behaviour could explain why the hydrophone tends to overestimate bedload fluxes when bedload fluxes are weak especially immediately downstream of a bar front (Fig. 9b).

Hydrophone lower detection limit was not reached during our study whereas the dispersion of bedload rates measured with samplers for low apparent bedload velocity (Fig. 3) suggests that the lower detection limit of the apparent bedload velocity by the aDcp seems to be about 1 $cm.s^{-1}$ (Rennie et al., 2017). This lower detection limit of the apparent bedload velocity should be reduced to the bottom track uncertainty by using our protocol with a submerged and fixed aDcp device.

6. Conclusions

In this work, direct (BTMA samplers), active (aDcp and DTM) and passive (hydrophone) acoustic measurements of bedload transport rates were compared in a large, sandy-gravel bed river characterized by the presence of bars and superimposed dunes. Calibration curves between apparent bedload velocity measured using aDcp and bedload rates measured using BTMA samplers were established but remain site-specific and dependent on grain

size. DTM seemed to be inappropriate where macroforms are present, as it influences the location and the size of superimposed mesoforms. The calculation of bedload rates with empirical formulas is sensitive to the bedload discharge coefficient for DTM and to thickness and concentration of active layer for aDcp. These parameters remain difficult to measure in the field. Results presented in this study highlight the potential of the hydrophone for the quantification and mapping of bedload transport rates in relatively large river channels where migrating bedforms are present. Previously hydrophones have mainly been used to monitor bedload transport rates in gravel-bed rivers. This study consolidates a recent study (Geay at al., 2020) by extending a general calibration curve to large sandy-gravel bed rivers. The hydrophone global calibration curve allows a good representation of the bedload fluxes evolution through a cross section. The method is more affordable to implement and more efficient than the reference method. This might allow mapping bedload transport rates by interpolating acoustic power along several cross sections performed on a large sandy gravel bed river. Moreover, acoustic devices (aDcp and hydrophone) are able to capture the evolution of bedload signal along bedforms stoss and lee sides with some limitation of bedform size for the hydrophone and signal noise for the aDcp. Regarding results of the comparison between bedload velocity and acoustic power, the association of aDcp and hydrophone could be an efficient way to control the quality of both devices. However, additional measurements and post-processing tasks are needed (Conevski et al., 2019) to explore the quality of the regression in other river environments (different grain sizes, river-bed slope or propagation effect).

562 **Appendices**

563 Appendix A: BTMA dataset
564

Date	Discharge ($m^3.s^{-1}$)	Measurements type	Number of BTMA sampling points	Number of BTMA samples	Mean unit bedload rate ($g.s^{-1}.m^{-1}$)	D_{50} (mm)	D_{90} (mm)
28/11/2016	1420	BTMA & DTM	3	50	38.1	0.8	3.0
29/11/2016	1460	BTMA & DTM	4	79	31.5	0.9	3.5
30/11/2016	1300	BTMA & DTM	4	80	33.2	0.8	2.9
01/12/2016	1100	BTMA & DTM	4	79	32.2	0.8	2.6
27/03/2017	687	BTMA. aDcp & DTM	4	80	25.3	0.7	2.9
28/03/2017	752	BTMA. aDcp & DTM	4	80	28.5	0.8	3.0
29/03/2017	827	BTMA. aDcp & DTM	4	57	29.0	0.8	3.8
30/03/2017	812	BTMA. aDcp & DTM	4	80	19.3	0.8	3.8
15/05/2017	346	BTMA. aDcp & DTM	3	60	6.3	0.9	4.8
16/05/2017	354	BTMA. aDcp & DTM	3	60	13.5	0.8	5.0
17/05/2017	401	BTMA. aDcp & DTM	3	55	9.0	0.9	4.7
18/05/2017	447	BTMA. aDcp & DTM	3	60	1.9	1.2	7.0
04/12/2017	243	BTMA & aDcp	3	60	1.8	1.1	7.4
05/12/2017	241	BTMA. aDcp & DTM	3	60	3.7	1.0	8.6
06/12/2017	243	BTMA. aDcp & DTM	3	60	6.6	1.2	6.7
07/12/2017	246	BTMA. aDcp & DTM	3	60	5.1	1.2	5.1
08/12/2017	226	BTMA. aDcp & DTM	3	60	5.0	1.6	7.9
15/01/2018	1740	BTMA. aDcp & DTM	3	60	61.4	1.0	2.9
16/01/2018	1550	BTMA. aDcp & DTM	3	60	89.4	0.9	2.8
17/01/2018	1460	BTMA. aDcp & DTM	4	80	53.2	0.8	3.0
18/01/2018	1540	BTMA. aDcp & DTM	4	80	97.7	1.0	3.3
19/01/2018	1510	BTMA. aDcp & DTM	3	60	55.6	0.8	2.6
30/01/2018	2410	BTMA. aDcp & DTM	3	60	68.6	0.8	2.3
31/01/2018	2290	BTMA. aDcp & DTM	3	59	55.8	0.8	2.2
08/02/2018	1550	BTMA. aDcp. DTM. Hydrophone	4	69	63.4	0.8	2.5
14/05/2018	443	BTMA. aDcp & DTM	4	79	2.2	0.9	2.7

15/05/2018	449	BTMA & aDcp	4	79	2.5	1.1	3.2
16/05/2018	547	BTMA. aDcp & DTM	3	60	6.6	1.2	4.4
17/05/2018	604	BTMA. aDcp. DTM. Hydrophone	3	60	7.2	1.2	4.4
15/04/2019	253	BTMA. aDcp & Hydrophone	3	60	22.1	0.9	3.3
16/04/2019	243	BTMA. aDcp & Hydrophone	3	60	22.1	1.1	5.1
17/04/2019	240	BTMA. aDcp & Hydrophone	3	60	24.9	1.2	3.7
18/04/2019	238	BTMA. aDcp & Hydrophone	3	58	16.4	1.0	5.3
27/05/2019	225	BTMA. aDcp. DTM. Hydrophone	1	26	34.6	1.0	4.8
29/05/2019	210	BTMA. aDcp. DTM. Hydrophone	1	28	22.0	1.1	3.3
09/12/2019	944	BTMA. aDcp. DTM. Hydrophone	2	40	29.1	0.7	2.5
10/12/2019	898	BTMA. aDcp. DTM. Hydrophone	3	60	20.1	0.6	2.5
11/12/2019	923	BTMA. aDcp. DTM. Hydrophone	3	45	34.9	0.8	2.4
12/12/2019	925	BTMA. aDcp. DTM. Hydrophone	2	37	26.4	0.7	2.7
19/12/2019	2050	BTMA. aDcp. DTM. Hydrophone	5	50	58.8	0.9	3.4
18/05/2020	514	BTMA & Hydrophone	1	57	19.7	0.9	2.8
19/05/2020	500	BTMA. aDcp & Hydrophone	2	79	30.9	1.0	2.6
20/05/2020	470	BTMA. aDcp & Hydrophone	4	40	14.5	-	-

565

566

Appendix B: ADcp dataset

Date	Number of aDcp sampling points *3	aDcp frequency (kHz)	aDcp type *1	Pulse type *2	Average aDcp sampling duration (s)	mean Va ($m.s^{-1}$)	mean water depth (m)	mean flow velocity ($m.s^{-1}$)
27/03/2017	4	1200	RG	BB	3909	0.013	2.0	0.7
28/03/2017	4	1200	RG	BB	3279	0.015	2.1	0.7
29/03/2017	4	1200	RG	BB	3276	0.011	2.2	0.7
30/03/2017	4	1200	RG	BB	1707	0.009	2.1	0.8
15/05/2017	3	1200	RG	BB	3018	0.002	1.3	0.8
16/05/2017	2	1200	RG	BB	2315	0.010	1.0	0.8
17/05/2017	3	1200	RG	BB	2618	0.003	1.4	0.8
18/05/2017	3	1200	RG	BB	2467	0.002	1.6	0.8
04/12/2017	3	1200	RG	BB	2647	0.000	1.2	0.7
05/12/2017	3	1200	RG	BB	2657	0.008	1.2	0.6
06/12/2017	3	1200	RG	BB	2246	0.000	1.2	0.7
07/12/2017	3	1200	RG	BB	2588	0.002	1.3	0.7
08/12/2017	3	1200	RG	BB	3400	0.003	1.2	0.6
15/01/2018	3	1200	RG	BB	3256	0.084	3.2	1.1
16/01/2018	3	1200	RG	BB	1800	0.058	2.9	1.0
17/01/2018	4	1200	RG	BB	3185	0.041	2.7	1.0
18/01/2018	4	1200	RG	BB	3656	0.055	2.8	1.0
19/01/2018	3	1200	RG	BB	2029	0.075	2.7	1.1
30/01/2018	3	1200	RG	BB	2138	0.051	3.9	1.1
31/01/2018	3	1200	RG	BB	2056	0.070	3.7	1.1
08/02/2018	4	3000	M9	BB	1136	0.038	2.8	0.9
14/05/2018	4	3000	M9	BB	2130	0.002	1.2	0.6
15/05/2018	4	variable	M9	HD	1133	0.011	1.5	0.6
16/05/2018	3	variable	M9	HD	948	0.002	1.4	0.7
17/05/2018	3	1200	RG	BB	1346	0.003	1.7	0.7
15/04/2019	3	variable	M9	HD	2601	0.009	1.2	0.8
16/04/2019	3	3000	M9	NB	1687	0.006	1.1	0.7
17/04/2019	3	variable	M9	HD	1152	0.010	1.0	0.7
18/04/2019	3	variable	M9	HD	3580	0.008	0.9	0.7

27/05/2019	1	3000	M9	NB	10949	0.003	0.9	0.8
29/05/2019	1	3000	M9	NB	11539	0.029	0.9	0.7
09/12/2019	2	3000	M9	NB	1753	0.023	1.7	0.8
10/12/2019	3	3000	M9	NB	1160	0.018	2.1	0.8
11/12/2019	3	3000	M9	NB	1288	0.027	1.6	0.9
12/12/2019	2	3000	M9	NB	1349	0.032	2.1	0.8
19/12/2019	5	3000	M9	NB	1221	0.056	3.0	1.1
19/05/2020	2	3000	M9	NB	7318	0.014	1.0	0.7
20/05/2020	4	3000	M9	NB	2988	0.004	1.6	0.7

*[1]: RG = aDcp Rio Grande RDI; M9 = aDcp M9 Sontek

*[2] BB = Broadband (coherent Pulse); NB = Narrowband (incoherent pulse); HD = Smartpulse HD

*[3] including sampling points with negative values.

573 Appendix C: DTM dataset
574

Date	Number of pairs of DTM profiles [*1]	average interval time DTM (min)	Number of dunes	Mean H_D (m)	Mean L_D (m)	Mean C_D ($m.d^{-1}$)
28/11/2016	2	18	65	0.19	2.88	43.0
29/11/2016	3	20	168	0.22	3.69	34.8
30/11/2016	3	18	121	0.24	4.16	37.6
01/12/2016	3	19	104	0.25	4.69	37.6
27/03/2017	3	38	132	0.13	3.13	28.3
28/03/2017	3	44	97	0.13	2.96	24.2
29/03/2017	3	43	117	0.14	3.25	25.7
30/03/2017	3	39	138	0.14	3.42	28.0
15/05/2017	3	65	20	0.04	2.17	18.1
16/05/2017	3	42	11	0.05	2.02	26.7
17/05/2017	3	38	18	0.05	2.01	28.0
18/05/2017	3	28	34	0.08	1.95	30.9
05/12/2017	1	73	48	0.13	2.90	17.9
06/12/2017	1	98	68	0.16	3.44	14.9
07/12/2017	1	72	63	0.17	3.62	17.3
08/12/2017	1	66	69	0.19	3.95	14.8
15/01/2018	6	23	228	0.32	6.66	38.1
16/01/2018	2	28	46	0.24	3.58	47.6
17/01/2018	3	32	52	0.25	4.36	34.9
18/01/2018	3	55	120	0.28	5.33	28.0
19/01/2018	3	31	110	0.26	4.95	31.4
30/01/2018	3	25	103	0.32	5.75	45.3
31/01/2018	4	22	83	0.28	5.02	45.4
08/02/2018	3	60	59	0.26	4.67	28.2
14/05/2018	6	35	58	0.06	2.92	20.8
16/05/2018	4	38	60	0.05	1.96	18.8
17/05/2018	6	34	81	0.05	1.98	22.3
27/05/2019	1	29	3	0.03	1.40	62.7
29/05/2019	1	26	7	0.03	1.28	30.7

09/12/2019	6	49	121	0.22	3.10	28.1
10/12/2019	6	42	227	0.17	3.60	33.2
11/12/2019	6	49	254	0.16	3.46	33.1
12/12/2019	6	50	297	0.18	3.82	35.9
19/12/2019	3	44	79	0.28	4.34	42.1

575 [*1] including profiles with less than 10 dunes or mean dune celerity which could not be calculated.

576

577 Appendix D: Hydrophone dataset

578

Date	Number of Hydrophone Drifts [*1]	average drift duration (s)	mean acoustic power (Pa^2)
08/02/2018	24	60	2.17E+13
17/05/2018	24	80	1.46E+12
15/04/2019	11	37	1.66E+12
16/04/2019	11	42	2.25E+12
17/04/2019	11	28	1.42E+12
18/04/2019	11	30	2.35E+12
27/05/2019	8	42	5.07E+11
29/05/2019	9	36	2.00E+12
09/12/2019	22	29	6.67E+12
10/12/2019	21	22	7.69E+12
11/12/2019	22	27	8.84E+12
12/12/2019	13	27	8.97E+12
19/12/2019	22	25	2.41E+13
18/05/2020	8	50	4.53E+12
19/05/2020	8	30	3.82E+12
20/05/2020	17	36	3.07E+12

579 [*1] including drifts which are not at the same location of BTMA sampling points.

580

Video supplement

Videos of BTMA sampling were added in supplement of this manuscript to appreciate the variability of bedload in the Loire River.

https://doi.org/10.5446/51563

https://doi.org/10.5446/51562

https://doi.org/10.5446/51561

https://doi.org/10.5446/51560

Author contribution

J. Le Guern prepared the manuscript with contributions from all co-authors. J. le Guern, T. Geay, A, Hauet, S. Zanker, S. Rodrigues elaborated the experimental protocol. T. Geay developed the hydrophone signal processing tools. A. Duperray P. Jugé, L. Vervynck, A. Hauet, S. Zanker, T. Geay, S. Rodrigues and J. Le Guern conducted the field surveys. A. Duperray P. Jugé, and L. Vervynck performed the bathymetry post-processing. S. Rodrigues and P. Tassi supervised this study. N. Claude helped in the analysis of BTMA and aDcp measurements.

Competing interests

The authors declare that they have no conflict of interest.

Acknowledgement

This study is a part of the Ph.D. thesis of the first author funded by the POI FEDER Loire (Convention no. 2017-EX002207) and Agence de l'Eau Loire Bretagne (decision no.2017C005), conducted in the frame of the Masterplan Plan Loire Grandeur Nature. We thank EDF DTG and ARD Intelligence des Patrimoines (Phase 2) for lending us acquisition equipment. Exagone Company is acknowledged for providing us data from Teria network, Voie Navigable de France (VNF) for their logistical support during field surveys and Polytech Tours. J.-P. Bakyono, P. Berault, T. Bulteau, B. Deleplancouille, Y. Guerez, T. Handfus, I. Pene and C. Wintenberger, are acknowledged for their help during field investigations and grain size analyses. We are grateful to T. Geay and J. Hugueny for the hydrophone treatment and aDcp data post-processing tools, respectively. The authors wish to thank Pr. K. M. Wantzen for checking the English quality of the manuscript.

606 **References**

607 Batalla, R. J.: Evaluation bed-material transport equations using field measurements in a sandy gravel-bed stream,
608 Arbùcies River, NE Spain, Earth Surf. Process. Landforms, 22 (2), 121-130, https://doi.org/10.1002/(SICI)1096-
609 9837(199702)22:2<121::AID-ESP671>3.0.CO;2-7, 1997.
610 Banhold, K., Schüttrumpf, H., Hillebrand, G. and Frings, R.: Underestimation of sand loads during bed-load
611 measurements- a laboratory examination, in: Proceedings of the international conference on Fluvial Hydraulics
612 (River Flow 2016), 11-14 July 2016, Saint Louis, USA, 2406 pp., 2016.
613 Barton, J., Slingerland, R. R. L., Pittman, S., and Gabrielson, T. B.: Monitoring coarse bedload transport with
614 passive acoustic instrumentation: A field study, US Geol. Surv. Sci. Investig. Rep., 38–51, 2010.
615 Bedeus, K., and Ivicsics, L.: Observation of the noise of bed load, Gen. Assem. Comm. Hydrom. Int. Assoc. Hydrol.
616 Sci. Berkeley, CA, USA, 19–31, 1963.
617 Bertoldi, W., Ashmore, P., and Tubino, M.: A method for estimating the mean bed load flux in braided rivers,
618 Geomorphology, 103, 330-340, https://doi.org/10.1016/j.geomorph.2008.06.014, 2009.
619 Best, J. L.: Sediment transport and bed morphology at river channel confluences, Sedimentology, 35, 481-498,
620 https://doi.org/10.1111/j.1365-3091.1988.tb00999.x, 1988.
621 Blanpain, O., Demoulin, X., Waeles, B., Ravilly, M., Garlan, T., and Guyomard, P.: Passive acoustic measurement
622 of bedload discharge features on a sandy seafloor, in: Proceedings of Seabed and Sediment Acoustics Volume 37
623 Part 1, Bath, United Kingdom, 7-9 september 2015.
624 Blott, S. J., and Pye, K.: GRADISTAT: A grain size distribution and statistics package for the analysis of
625 unconsolidated sediments, Earth Surf. Process. Landforms, 26 (11), 1237-1248, https://doi.org/10.1002/esp.261,
626 2001.
627 Boiten, W.: Hydrometry, IHE Delft Lecture Note Series, A.A. Balkema Publishers, Netherland, 256 pp,
628 https://doi.org/10.1201/9780203971093, 2003.
629 Brasington, J., Rennie, C. D., Vericat, D., Williams, R., Goodsell, B., Hicks, M., and Batalla, R.: Monitoring braided
630 river morphodynamics with an acoustic Dopler current profiler, in: Proceedings of the 34th World Congress of the
631 International Association for Hydro-Environment Research and Engineering: 33rd Hydrology and Water Resources
632 Symposium and 10th Conference on Hydraulics in Water Engineering, Brisbane, 3396-3403, 2011.
633 Carling, P. A., Williams, J. J., Gölz, E., and Kelsey, A. D.: The morphodynamics of fluvial sand dunes in the River
634 Rhine, near Mainz, Germany. II. Hydrodynamics and sediment transport, Sedimentology, 47, 253-278,
635 https://doi.org/10.1046/j.1365-3091.2000.00291.x, 2000.
636 Church, M., and Haschenburger, J. K.: What is the “active layer”?, Water Resour. Res., 53 (1), 5-10,
637 https://doi.org/10.1002/2016WR019675, 2017.

638 Claude, N., Rodrigues, S., Bustillo, V., Bréhéret, J. G., Macaire, J. J., and Jugé, P.: Estimating bedload transport
639 in a large sand-gravel bed river from direct sampling, dune tracking and empirical formulas, Geomorphology, 179,
640 40-57, https://doi.org/10.1016/j.geomorph.2012.07.030, 2012.
641 Claude, N., Rodrigues, S., Bustillo, V., Bréhéret, J. G., Tassi, P., and Jugé, P.: Interactions between flow structure
642 and morphodynamic of bars in a channel expansion/contraction, Loire River, France, Water Resour. Res., 50,
643 https://doi.org/10.1002/2013WR015182, 2014.
644 Conevski, S.: Bedload Monitoring by means of Hydro-Acoustic Techniques, Ph.D. thesis, Norwegian University of
645 Science and Technology, Norway, 200 pp., 2018.
646 Conevski, S., Guerrero, M., Ruther N.,and Rennie, C. D.: Laboratory investigation of apparent bedload velocity
647 measured by ADCPs under different transport conditions, J. Hydraul. Eng., 145 (11),
648 https://doi.org/10.1061/(ASCE)HY.1943-7900.0001632, 2019.
649 Conevski, S., Guerrero, M., Winterscheid, A., Rennie, C. D., and Ruther N.: Acoustic sampling effects on bedload
650 quantification using acoustic Doppler current profilers, Journal of Hydraulic Research,
651 https://doi.org/10.1080/00221686.2019.1703047, 2020a.
652 Conevski, S., Guerrero, M., Rennie, C. D., and Ruther, N.: Towards an evaluation of bedload transport
653 characteristics by using Doppler and backscatter outputs from ADCPs, Journal of Hydraulic Research,
654 https://doi.org/10.1080/00221686.2020.1818311, 2020b.
655 Cordier, F., Tassi, P., Claude, N., Crosato, A., Rodrigues, S., and Pham Van Bang, D.: Bar pattern and sediment
656 sorting in channel contraction/expansion area: Application to the Loire River at Bréhémont (France), Advances in
657 Water Resources, 140, https://doi.org/10.1016/j.advwatres.2020.103580, 2020.
658 de Vries, M.: Information on the Arnhem Sampler (BTMA), Internal Report n°3-79, Delft University of Technology,
659 Department of Civil Engineering, Fluid Mechanics Group, 1979.
660 Eijkelkamp: Operating instructions: Bedload Transport Meter Arnhem, Giesbeek, Netherland, 8 pp., 2003.
661 Engel, P., and Lau, Y. L.: Computation of Bed Load Using Bathymetric Data, Journal of the Hydraulics Division,
662 106 (3), 369-380, 1980.
663 Folk, R. L., and Ward, W. C.: Brazos River bar (Texas); a study in the significance of grain size parameters, Journal
664 of Sedimentary Research, 27 (1), 3-26, https://doi.org/10.1306/74D70646-2B21-11D7-8648000102C1865D, 1957.
665 Frings, R. M., and Vollmer, S.: Guidelines for sampling bed-load transport with minimum uncertainty,
666 Sedimentology, 64 (6), 1630-1645, https://doi.org/10.1111/sed.12366, 2017.
667 Frings, R. M., Gehres, N., Promny, M., Middelkoop, H., Schüttrumpf, H., and Vollmer, S.: Today's sediment budget
668 of the Rhine River channel, focusing on the Upper Rhine Graben and Rhenish Massif, Geomorphology, 204, 573-
669 587, https://doi.org/10.1016/j.geomorph.2013.08.035, 2014.
670 Gaeuman, D., and Jacobson, R. B.: Acoustic bed velocity and bed load dynamics in a large sand bed river, J.
671 Geophys. Res., 111, F02005, https://doi.org/10.1029/2005JF000411, 2006.

672 Gaeuman, D., and Jacobson, R. B.: Field Assessment of Alternative Bed-Load Transport Estimators, J. Hydraul.
673 Eng., 133 (12), 1319-1328, https://doi.org/10.1061/(ASCE)0733-9429(2007)133:12(1319), 2007.
674 Gaeuman, D., and Pittman, S.: Relative Contributions of Sand and Gravel Bedload Transport to Acoustic Doppler
675 Bed-Velocity Magnitudes in the Trinity River, California, U.S. Geological Survey Scientific Investigations Report,
676 2010-5091, 2010.
677 Gaweesh, M. T. K., and van Rijn, L. C.: Bed-load sampling in sand-bed rivers, J. Hydraul. Eng., 120 (12), 1364-
678 1384, https://doi.org/10.1061/(ASCE)0733-9429(1994)120:12(1364), 1994.
679 Geay, T., Belleudy, P., Gervaise, C., Habersack, H., Aigner, J., Kreisler, A., Seitz, H., and Laronne, J. B.: Passive
680 acoustic monitoring of bed load discharge in a large gravel bed river, J. Geophys. Res.: Earth Surf., 122 (2),
681 https://doi.org/10.1002/2016JF004112, 2017.
682 Geay, T., Michel, L., Zanker, S., and Rigby, J. R.: Acoustic wave propagation in rivers: an experimental study. Earth
683 Surface Dynamics, 7 (2), 537–548, https://doi.org/10.5194/esurf-7-537-2019, 2019.
684 Geay, T., Zanker, S., Misset, C., and Recking, A.: Passive Acoustic Measurement of Bedload Transport: Toward
685 a Global Calibration Curve?, J. Geophys. Res.: Earth Surf., 125 (8), https://doi.org/10.1029/2019JF005242, 2020.
686 Gimbert, F., Fuller, B. M., Lamb, M. P., Tsai, V. C., and Johnson, J. P. L.: Particle transport mechanics and induced
687 seismic noise in steep flume experiments with accelerometer-embedded tracers, Earth Surf. Process. Landforms,
688 44, 219-241, https://doi.org/10.1002/esp.4495, 2019.
689 Gray, J. R., Gartner, J. W., Barton, J. S., Gaskin, J., Pittman, S. A., and Rennie, C. D.: Surrogate Technologies for
690 Monitoring Bed-Load Transport in Rivers, Sedimentology of Aqueous Systems, 46-79,
691 https://doi.org/10.1002/9781444317114.ch2, 2010.
692 Grill, G., Lehner, B., Thieme, M. et al.: Mapping the world's free-flowing rivers. Nature 569, 215–221,
693 https://doi.org/10.1038/s41586-019-1111-9, 2019.
694 Hilldale, R. C., Goodwiller, B. T., Carpenter, W. O., and Chambers, J. P.: Measuring Coarse Bed Load Using
695 Hydrophones, Closeout report, Reclamation Managing Water in the West, 2014.
696 Holmes, R. R. Jr.: Measurement of Bedload Transport in Sand-Bed Rivers: A Look at Two Indirect Sampling
697 Methods, U.S. Geological Survey Scientific Investigations Report, 2010-5091, 2010.
698 Jackson, R. G.: Hierarchical attributes and a unifying model of bed forms composed of cohesionless material and
699 produced by shearing flow, Geological Society of America Bulletin, 86, 1523-1533, 1975.
700 Jamieson, E. C., Rennie, C. D., Jacobson, R. B., and Townsend, R. D.: Evaluation of ADCP Apparent Bed Load
701 Velocity in a large Sand-Bed River: Moving versus Stationary Boat Conditions, J. Hydraul. Eng., 137, 1064-1071,
702 https://doi.org/10.1061/(ASCE)HY.1943-7900.0000373, 2011.
703 Kenney, T. A. (2006), Cross-sectional progression of apparent bedload velocities, in: Proceedings of the Eighth
704 Federal Interagency Sedimentation Conference (8th FISC), April 2–6 2006, Reno, Nevada, USA, 8 pp., 2006.

Kondolf, G. M., Schmitt, R. J. P., Carling, P., et al.: Changing sediment budget of the Mekong: Cumulative threats and management strategies for a large river basin. Sci Total Environ., 625, 114-134, https://doi.org/10.1016/j.scitotenv.2017.11.361, 2018.

Kostaschuk, R., and Villard, P.: Flow and sediment transport over large subaqueous dunes: Fraser River, Canada, Sedimentology, 43 (5), 849-863, https://doi.org/10.1111/j.1365-3091.1996.tb01506.x, 1996.

Kostaschuk, R., Best, J., Villard, P., Peakall, J., and Franklin, M.: Measuring flow velocity and sediment transport with an acoustic Doppler current profiler, Geomorphology, 68, 25-37, https://doi.org/10.1016/j.geomorph.2004.07.012, 2005.

Latosinski, F. G., Szupiany, R. N., Guerrero, M., Amsler, M. L., and Vionnet, C.: The ADCP's bottom track capability for bedload prediction: Evidence on method reliability from sandy river applications, Flow Measurement and Instrumentation, 54, 124-135, https://doi.org/10.1016/j.flowmeasinst.2017.01.005, 2017.

Leary, K. C. P., and Buscombe, D.: Estimating sand bed load in rivers by tracking dunes: a comparison of methods based on bed elevation time series, Earth Surf. Dynam., 8, 161-172, https://doi.org/10.5194/esurf-8-161-2020, 2020.

Le Guern, J., Rodrigues, S., Tassi, P., Jugé, P., Handfus, T., Duperray, A., and Berrault, P.: Influence of migrating bars on dune geometry, in: Book of Abstracts of the 6th Marine and River Dune Dynamics conference, 1-3 April 2019, Bremen, Germany, 157-160, 2019a.

Le Guern, J., Rodrigues, S., Tassi, P., Jugé, P., Handfus, T., and Duperray, A.: Initiation, growth and interactions of bars in a sandy-gravel bed river, in: Book of Abstracts of the 11th Symposium on River, Costal and Estuarine Morphodynamics, 16-21 November 2019, Auckland, New-Zealand, 226 pp., 2019b.

Marineau, M. D., Wright, S. A., and Gaeuman, D.: Calibration of sediment-generated noise measured using hydrophones to bedload transport in the Trinity River, California, USA, in: Proceeding of River Flow 2016 - eighth International Conference on Fluvial Hydraulics, Saint Louis, USA, 12-15 July 2016, 1519–1526, 2016.

Mendoza, A., Abad, J. D., Langendoen, E. J., Wang, D., Tassi, P., and El Kadi Abderrezzak, K.: Effect of Sediment Transport Boundary conditions on the Numerical Modeling of Bed Morphodynamics, J. Hydraul. Eng., 143 (4), https://doi.org/10.1061/(ASCE)HY.1943-7900.0001208, 2017.

Nittrouer, J. A., Allison, M. A., and Campanella, R.: Bedform transport rates for the lowermost Mississippi River, J. Geophys. Res., 113, F03004, https://doi.org/10.1029/2007JF000795, 2008.

Peters, J. J.: Discharge and Sand Transport in the Braided Zone of the Zaire Estuary, Netherlands Journal of Sea Research, 12, 273-292, https://doi.org/10.1016/0077-7579(78)90031-5, 1978.

Ramooz, R., and Rennie, C. D.: Laboratory Measurement of Bedload with an ADCP, U.S. Geological Survey Scientific Investigations Report, 2010-5091, 2010.

Reesink, A. J. H., Parsons, D. R., and Thomas, R. E.: Sediment transport and bedform development in the lee of bars: Evidence from fixed- and partially-fixed bed experiments, in: Proceeding of River Flow 2014 - seventh International Conference on Fluvial Hydraulics, Lausanne, Switzerland, 3-5 Septembre 2014, 8 pp., 2014.

Rennie, C. D., and Millar, R. G.: Measurement of the spatial distribution of fluvial bedload transport velocity in both sand and gravel, Earth Surf. Process. Landforms, 29, 1173-1193, doi:10.1002/esp.1074, 2004.

Rennie, C. D., and Villard, P. V.: Site specificity of bed load measurement using an acoustic Doppler current profiler, J. Geophys. Res., 109, F03003, https://doi.org/10.1029/2003JF000106, 2004.

Rennie, C. D., Millar, R. G., and Church, M. A.: Measurement of Bed Load Velocity using an Acoustic Doppler Current Profiler, J. Hydraul. Eng., 128 (5), 473-483, https://doi.org/10.1061/(ASCE)0733-9429(2002)128:5(473), 2002.

Rennie, C. D., Vericat, D., Williams, R. D., Brasington, J., and Hicks, M.: Calibration of acoustic doppler current profiler apparent bedload velocity to bedload transport rate, in: Gravel-Bed Rivers: Processes and Disasters, Oxford, UK: Wiley Blackwell, 209–233, https://doi.org/10.1002/9781118971437.ch8, 2017.

Rodrigues, S., Mosselman, E., Claude, N., Wintenberger, C. L., and Jugé, P.: Alternate bars in a sandy gravel bed river: generation, migration and interactions with superimposed dunes, Earth Surf. Process. Landforms, 40 (5), 610-628, https://doi.org/10.1002/esp.3657, 2015.

Simons, D. B., Richardson, E. V., and Nordin, C. F. Jr.: Bedload Equation for Ripples and Dunes, U.S. Geol. Survey Prof. Paper, 462-H, https://doi.org/10.3133/pp462H, 1965.

Syvitski, J. P. M., and Milliman, J. D.: Geology, Geography, and Humans Battle for Dominance over the Delvery of Fluvial Sediment to the Coastal Ocean, The Journal of Geology, 15(1), 1-19, https://doi.org/10.1086/509246, 2007.

Ten Brinke, W. B. M., Wilbers, A. W. E., and Wesseling, C.: Dune growth, decay and migration rates during a large-magnitude flood at a sand and mixed sand-gravel bed in the Dutch Rhine river system, in: In Fluvial Sedimentology VI, Vol. 28 of Special Publications of the International Association of Sedimentologists, 15-32, https://doi.org/10.1002/9781444304213.ch2, 1999.

Thorne, P. D., Heathershaw, A. D., and Troiano, L.: Acoustic Detection of Seabed Gravel Movement in Turbulent Tidal Currents, Marine Geology, 54, M43-M48, https://doi.org/10.1016/0025-3227(84)90035-5, 1984.

Thorne, P. D.: The measurement of acoustic noise generated by moving artificial sediments, J. Acoust. Soc. Am., 78 (3), 1013–1023, https://doi.org/10.1121/1.393018, 1985.

Thorne, P. D.: Laboratory and marine measurements on the acoustic detection of sediment transport, J. Acoust. Soc. Am., 80(3), 899, https://doi.org/10.1121/1.393913, 1986.

Thorne, P. D.: An overview of underwater sound generated by interparticle collisions and its application to the measurements of coarse sediment bedload transport, Earth Surf. Dyn., 2 (2), 531–543, https://doi.org/10.5194/esurf-2-531-2014, 2014.

Van den Berg, J. H.: Bedform migration and bed-load transport in some rivers and tidal environments, Sedimentology, 34, 681-698, https://doi.org/10.1111/j.1365-3091.1987.tb00794.x, 1987.

Van der Mark, C. F., and Blom, A.: A new and widely applicable tool for determining the geometric properties of bedforms, Civil Engineering & Manageement Research Report 2007R-003/WEM-002 ISSN 1568-4652, University of Twente, Enschede, Netherlands, 57 pp., 2007.

Van Rijn, L. C.: Sediment Transport. Part I: Bed Load Transport, J. Hydraul. Eng., 110, 1431-1456, https://doi.org/10.1061/(ASCE)0733-9429(1984)110:10(1431), 1984.

Van Rijn, L. C., and Gaweesh, M. T. K.: New Total Sediment-Load Sampler, J. Hydraul. Eng., 118 (12), 1686–1691. https://10.1061/(ASCE)0733-9429(1992)118:12(1686), 1992.

Villard, P. V., and Church, M.: Bar and dune development during a freshet: Fraser River Estuary, British Colombia, Canada, Sedimentology, 52, 737-756, https://doi.org/10.1111/j.1365-3091.2005.00721.x, 2005.

Villard, P., Church, M., and Kostaschuk, R.: Estimating bedload in sand-bed channels using bottom tracking from an acoustic Doppler profiler, Spec. Publs int. Ass. Sediment, 35, 197-209, https://doi.org/10.1002/9781444304350.ch12, 2005.

Vörösmarty, C., McIntyre, P., Gessner, M., Dudgeon, D., Prusevich, A., Green, P., Glidden, S., Bunn, S. E., Sullivan, C. A., Reidy Liermann, C., and Davies, P. M.: Global threats to human water security and river biodiversity, Nature, 467, 555–561, https://doi.org/10.1038/nature09440, 2010.

Wilbers, A.: The development and hydraulic roughness of subaqueous dunes, Neth. Geogr. Stud, Fac. of Geosci., Utrecht Univ., Utrecht, Netherlands. 323, 224 pp., 2004.

Williams, R. D., Rennie, C. D., Brasington, J., Hicks, D. M., and Vericat, D.: Linking the spatial distribution of bed load transport to morphological change during high-flow events in shallow braided river, J. Geophys. Res. Earth Surf., 120, 604–622, https://doi.org/10.1002/2014JF003346, 2015.